EUROPEAN ORGANIZATION FOR NUCLEAR RESEARCH

CERN-EP/2000-104
July 24, 2000

Measurement of the W-Pair Production Cross Section and W-Decay Branching Fractions in e^+e^- Interactions at $\sqrt{s} = 189$ GeV

The L3 Collaboration

Abstract

The data collected by the L3 experiment at LEP at a centre-of-mass energy of 188.6 GeV are used to measure the W-pair production cross section and the W-boson decay branching fractions. These data correspond to an integrated luminosity of 176.8 pb^{-1}. The total cross section for W-pair production, combining all final states, is measured to be $\sigma_{\mathrm{WW}} = 16.24 \pm 0.37\ (stat.) \pm 0.22\ (syst.)$ pb. Including our data collected at lower centre-of-mass energies, the hadronic branching fraction of the W-boson is determined to be $B(\mathrm{W} \rightarrow \mathrm{qq}) = [68.20 \pm 0.68\ (stat.) \pm 0.33\ (syst.)]\ \%$. The results agree with the Standard Model predictions.

Submitted to *Phys. Lett. B*

1 Introduction

Since 1996 the electron-positron collider LEP at CERN has exceeded the centre-of-mass energy required to produce W bosons in pairs, $\mathrm{e^+e^-} \rightarrow \mathrm{W^+W^-}$. To lowest order within the Standard Model [1, 2] (SM), three Feynman diagrams contribute to W-pair production: s-channel γ and Z-boson exchange and t-channel ν_e exchange, referred to as CC03 [3–5]. The W boson decays into a quark-antiquark pair, for example $\mathrm{W^-} \rightarrow \bar{\mathrm{u}}\mathrm{d}$ or $\bar{\mathrm{c}}\mathrm{s}$, or a lepton-antilepton pair, $\mathrm{W^-} \rightarrow \ell^-\bar{\nu}_\ell$ ($\ell = \mathrm{e}, \mu, \tau$), in the following denoted as qq, $\ell\nu$ or ff in general for both $\mathrm{W^+}$ and $\mathrm{W^-}$ decays.

In 1998 the L3 detector [6] collected an integrated luminosity of 176.8 $\mathrm{pb^{-1}}$ [7,8] at a centre-of-mass energy, $\sqrt{s}$, of 188.6 GeV, increasing our total W-pair statistics by a factor of four. Cross sections are measured for all four-fermion final states arising in W-pair production. The total W-pair production cross section is determined in a combined analysis. For the W-decay branching fractions, the results are combined with our previous measurements [9].

2 Analysis of W-Pair Production

The selections of W-pair events are based on the four-fermion final states from W-pair decays: $\ell\nu\ell\nu(\gamma)$, $\mathrm{qqe}\nu(\gamma)$, $\mathrm{qq}\mu\nu(\gamma)$, $\mathrm{qq}\tau\nu(\gamma)$ and $\mathrm{qqqq}(\gamma)$. Additional contributions to the production of these final states from other neutral-current (NC) or charged-current (CC) Feynman diagrams are small. At the current level of statistical accuracy the interference effects need to be taken into account only for $\mathrm{e^+e^-} \rightarrow \ell\nu\ell\nu(\gamma)$ (CC56+NC56) and $\mathrm{e^+e^-} \rightarrow \mathrm{qqe}\nu(\gamma)$ (CC20) [3–5].

The selection criteria are similar to those used for the data collected at $\sqrt{s} = 183$ GeV in 1997 [9] but are adapted to the higher centre-of-mass energy. In the following, only the main ideas and important changes are described. Particular emphasis is placed on the evaluation of systematic uncertainties.

For the identification of electrons, an energy deposition in the electro-magnetic calorimeter is required, matched in azimuth with a track reconstructed in the central tracking system. Muons are identified either as a track reconstructed in the muon chambers pointing back to the interaction vertex or by their minimum-ionising-particle (MIP) signature in the central tracking system and calorimeters. Hadronic jets arising from τ decays are identified using a neural network based on topological variables: the number of tracks and calorimetric clusters associated to the jet, the half-opening angle of the jet, its electro-magnetic energy and its mass. The jet clustering algorithm for a hadronically decaying τ is based on geometrical clustering inside a cone of 15° half-opening angle [10]. For all other jets the Durham algorithm [11] is used. The sum of the four-momenta of the neutrinos in semileptonic, $\mathrm{e^+e^-} \rightarrow \mathrm{qq}\ell\nu(\gamma)$, and leptonic, $\mathrm{e^+e^-} \rightarrow \ell\nu\ell\nu(\gamma)$, events is identified with the missing four-momentum of the event.

The following event generators are used to simulate the signal and background processes: KORALW [12], HERWIG [13] and ARIADNE [14] ($\mathrm{e^+e^-} \rightarrow \mathrm{WW} \rightarrow \mathrm{ffff}(\gamma)$); EXCALIBUR [15] ($\mathrm{e^+e^-} \rightarrow \mathrm{ffff}(\gamma)$); PYTHIA [16] ($\mathrm{e^+e^-} \rightarrow \mathrm{q\bar{q}}(\gamma), \mathrm{ZZ}(\gamma), \mathrm{WW}(\gamma)$); KK2F [17] ($\mathrm{e^+e^-} \rightarrow \mathrm{q\bar{q}}(\gamma)$); KORALZ [18] ($\mathrm{e^+e^-} \rightarrow \mu^+\mu^-(\gamma)$, $\tau^+\tau^-(\gamma)$); BHAGENE3 [19] and BHWIDE [20] ($\mathrm{e^+e^-} \rightarrow \mathrm{e^+e^-}(\gamma)$); TEEGG [21] ($\mathrm{e^+e^-} \rightarrow \mathrm{e^+e^-}\gamma(\gamma)$); DIAG36 [22] (leptonic two-photon collisions) and PHOJET [23] (hadronic two-photon collisions). The response of the L3 detector is modelled with the GEANT [24] detector simulation program which includes the effects of energy loss, multiple scattering and showering in the detector materials and in the beam pipe. Time dependent detector inefficiencies are taken into account in the simulation. The selection efficiencies are derived from Monte Carlo simulations fixing the mass and the width of the W boson to $m_{\mathrm{W}} = 80.50$ GeV and $\Gamma_{\mathrm{W}} = 2.11$ GeV, respectively.

2.1 $e^+e^- \rightarrow \ell\nu\ell\nu(\gamma)$

The event selection for the process $e^+e^- \rightarrow \ell\nu\ell\nu(\gamma)$ requires two high energy acoplanar leptons with large missing energy due to the neutrinos. The selection depends on whether the event contains zero, one or two identified electrons or muons, referred to as jet-jet, lepton-jet and lepton-lepton classes, where jet denotes a hadronic τ-jet. The electron identification is improved by including also the SPACAL calorimeter that covers the polar angular region between the barrel and the end-cap BGO calorimeters.

A total of 190 events is selected: 116 lepton-lepton events, 64 lepton-jet events and 10 jet-jet events. The distribution of the energy of the highest-energy lepton in the lepton-lepton class and the distribution of the selected events in the different reconstructed final-state topologies are shown in Figure 1.

The signal efficiencies are determined with four-fermion (CC56+NC56) Monte Carlo samples and are quoted for the following phase-space cuts: $|\cos\theta| < 0.96$ for both charged leptons, where θ is the polar angle with respect to the beam axis, and energies greater than 15 GeV and 5 GeV for the higher and the lower energy lepton, respectively. Table 1 lists these efficiencies in the form of a 6-by-6 matrix, relating $\ell\nu\ell\nu$ events at generated four-fermion level to $\ell\nu\ell\nu$ events identified at reconstruction level. The overall selection efficiency in the full phase-space, based on a W-pair (CC03) Monte Carlo and under the assumption of charged-current lepton universality in W decays, is 52.3%. The background contributions, dominated by leptonic two-photon collisions and $e^+e^- \rightarrow \ell^+\ell^-(\gamma)$ events, are listed in Table 2.

2.2 $e^+e^- \rightarrow qq\ell\nu(\gamma)$

The selection of $e^+e^- \rightarrow qq\ell\nu(\gamma)$ events requires an identified high energy lepton, two hadronic jets with high particle multiplicity and missing momentum due to one or more neutrinos. The neutrino four-momentum vector is constructed by using the missing three-momentum vector, taken to be massless. In order to separate $qqe\nu(\gamma)$ and $qq\mu\nu(\gamma)$ events from $qq\tau\nu(\gamma)$ events for the case of a leptonic τ decay, the effective mass of the lepton-neutrino system is used. In the case of the $W \rightarrow e\nu$ and $W \rightarrow \mu\nu$ decay modes, the effective mass is peaked around the W mass, whereas for $W \rightarrow \tau\nu$ decays its value is typically much lower. The cut position is chosen such that the correlation among the cross sections of the three final states is minimised. The selection efficiencies and the background contaminations, dominated by $q\bar{q}(\gamma)$ events, are presented in Tables 1 and 2.

The $qqe\nu(\gamma)$ selection accepts 363 events. The distributions of the energy of the electron and of the electron-neutrino invariant mass are shown in Figure 1. The signal efficiency for $qqe\nu(\gamma)$ events is determined from a four-fermion (CC20) Monte Carlo sample within the following phase-space cuts: $E_{\mathrm{e}}, E_\nu > 15$ GeV, where E_{e} and E_ν are the electron and neutrino energies; $|\cos\theta_{\mathrm{e}}|, |\cos\theta_\nu| < 0.98$, where θ_{e} and θ_ν are the electron and neutrino polar angles; $M_{\mathrm{e}\nu}, M_{\mathrm{qq}} >$ 45 GeV, where $M_{\mathrm{e}\nu}$ and M_{qq} are the electron-neutrino and quark-quark invariant masses. These values are changed with respect to our previous analysis due to the increased centre-of-mass energy.

A total of 340 events are accepted by the $qq\mu\nu(\gamma)$ selection: 299 candidates with a muon reconstructed in the muon spectrometer and 41 with a muon identified by its MIP signature. The distributions of the momentum of the muon and of the variable $\alpha \sin\theta_\nu$, which discriminates against the $q\bar{q}(\gamma)$ background events, are presented in Figure 2. The angle α is that between the direction of the muon and the nearest hadronic jet and θ_ν is the polar angle of the neutrino.

A total of 329 $qq\tau\nu(\gamma)$ events are selected: 53 $\tau \rightarrow \nu e\bar{\nu}$, 50 $\tau \rightarrow \nu\mu\bar{\nu}$ and 226 $\tau \rightarrow \nu+$hadrons candidates. The distributions of the jet-jet invariant mass and of the visible τ energy are shown in Figure 2.

2.3 $e^+e^- \rightarrow qqqq(\gamma)$

The $e^+e^- \rightarrow qqqq(\gamma)$ selection requires high multiplicity four-jet events with low missing energy. It accepts 94.8% of the $WW \rightarrow qqqq(\gamma)$ signal with a purity of 48.4%, corresponding to 2674 selected events. The measurement of jet energies and angles is improved by a kinematic fit that imposes four-momentum conservation.

A neural network is trained to further separate the signal from the main $e^+e^- \rightarrow q\bar{q}(\gamma)$ background, which is actually dominated by events with multi-gluon radiation. The input to the network consists of ten event variables: minimal and maximal jet energy, the energy difference between the two remaining jets, the minimal jet cluster multiplicity, the logarithm of the Durham jet-resolution parameter y_{34} at which the event changes from a four-jet to a three-jet topology, the spherocity [25], the sum of the cosines of the jet-jet angles, the probability of the kinematic fit and the jet broadening of the most and least energetic jets. The jet broadening is defined as $\sum \sqrt{p_t} / \sum \sqrt{p}$ where the sum is over the particles belonging to the jet, p_t is the transverse momentum relative to the reconstructed jet axis and p is the momentum of the particle. The distributions of four of these variables are shown in Figure 3. The network is trained such that its output peaks at one for the signal and at zero for the background, as shown in Figure 4.

The neural network output distribution for data events is fitted by a linear combination of outputs derived from Monte Carlo simulations for signal and background. A binned maximum likelihood fit is performed leaving both the signal and the most significant background ($e^+e^- \rightarrow q\bar{q}(\gamma)$) cross sections as free parameters. The latter is measured as 104.9 ± 3.4 pb, in agreement with both our measurement [8] and the SM value of 96.9 pb.

3 Systematic Uncertainties

The systematic uncertainties taken into account in the determination of the results are summarised in Table 3. Common to all final states is the uncertainty on the integrated luminosity of 0.2% [8]. The Monte Carlo statistics for both signal and background processes affects mainly the $\ell\nu\ell\nu(\gamma)$ final states.

The uncertainty due to the selection procedure is evaluated by varying the positions of the selection cuts and interpreting the corresponding changes in the measured cross sections as systematic uncertainties. The systematic uncertainty on the neural network output in the $qqqq(\gamma)$ selection is estimated by recalculating the input variables of the neural network after smearing and scaling the measurements of energy depositions and tracks in the simulation according to the uncertainty on their resolutions. In all selections, consistent results are found by studying the change in efficiency due to variations of the detector calibration within its uncertainty. The calibration is studied using samples of di-lepton and di-jet events, collected during the calibration runs at $\sqrt{s} = 91$ GeV and at higher energies. The trigger inefficiency as well as its uncertainty is found to be negligible. The systematic uncertainty assigned to the selection procedure is in the range 1.1% to 2.5% depending on the final state.

The theoretical uncertainties on the background cross sections, mainly on hadronic two-photon collisions (50%) and neutral-current four-fermion processes (5%), are propagated to the W-pair cross sections. The observed change of 0.1% to 0.3% is assigned as a systematic uncertainty. The KK2F Monte Carlo generator, instead of PYTHIA, is also used to simulate the $q\bar{q}(\gamma)$ background revealing no significant deviation on the measured cross section.

The dependence of the selection efficiencies on the mass and width of the W boson is studied using Monte Carlo samples simulated with different m_W and Γ_W values. The propagation of the world average uncertainties on these two parameters [26], 100 MeV on m_W and 60 MeV on Γ_W, is taken as a systematic uncertainty and ranges from 0.1% to 0.3%.

The systematic uncertainty on initial-state radiation (ISR) due to its approximate (leading-log) treatment in KORALW is investigated by reweighting the energy and transverse momentum spectra of the ISR photons. This is done according to an exact $\mathcal{O}(\alpha)$ matrix element calculation [27] that also includes leading $\mathcal{O}(\alpha^2)$ contributions at small angles. This study shows that the associated systematic uncertainty on the cross section determination is negligible. For the $\ell\nu\ell\nu(\gamma)$ and $qqe\nu(\gamma)$ selections, the efficiencies are determined by using EXCALIBUR Monte Carlo events. To estimate the systematic uncertainty due to the restriction in the EXCALIBUR program to strictly collinear ISR photons, the KORALW generator, which includes both collinear and non-collinear ISR photons, is used. The change in the selection efficiency of KORALW events given by including or removing the non-collinear contribution is used as an estimate of the similar effect of neglecting such photons in EXCALIBUR. The $\ell\nu\ell\nu(\gamma)$ selection, requiring low activity in the regions of the detector away from the leptons, is sensitive to the transverse momentum of radiated photons. The resulting reduction of 0.5% absolute is applied as a correction to the EXCALIBUR efficiency and it is included in the results reported in Table 1. For the $qqe\nu(\gamma)$ final state, the correction turns out to be negligible. The total uncertainty on the correction in the $\ell\nu\ell\nu(\gamma)$ case, propagated to the cross section, amounts to 0.2% and is assigned as the systematic uncertainty due to ISR.

Final-state radiation (FSR) is absent in EXCALIBUR while it is implemented in KORALW by using the PHOTOS package [28] based on the leading-log approximation. A similar procedure as for ISR is then applied using the KORALW program to correct the efficiencies for the complete absence of FSR in EXCALIBUR in the case of the $\ell\nu\ell\nu(\gamma)$ and $qqe\nu(\gamma)$ selections. The correction amounts to a reduction in efficiency of 0.4% absolute for the $\ell\nu\ell\nu(\gamma)$ and 1.3% absolute for the $qqe\nu(\gamma)$ final states and is included in the results listed in Table 1. The effect on the $qqe\nu(\gamma)$ selection comes from its sensitivity to the electron isolation requirements affected by FSR photons. The PHOTOS package is inaccurate in the hard non-collinear region [28]. The related systematic uncertainty is estimated by determining the selection efficiencies using Monte Carlo signal events containing soft radiative photons only. Half of the difference with respect to the full radiation simulation, ranging from 0.2% to 0.9%, is taken as a systematic uncertainty.

The determination of the efficiency for the $qq\mu\nu(\gamma)$ and $qq\tau\nu(\gamma)$ selections, as well as the neural network output shape for the $qqqq(\gamma)$ channel, is based on a W-pair (CC03) Monte Carlo sample. This Monte Carlo neglects non-WW contributions interfering with the CC03 diagrams. In order to study the effect on the cross section, the CC03 Monte Carlo events are reweighted by the squared matrix element ratio of the full four-fermion calculation to the CC03 one. In the case of $qqqq(\gamma)$ selection, this reweighting procedure takes into account that the $ZZ(\gamma)$ final states are treated in the background subtraction. The difference in accepted cross section, in the range 0.1% to 0.4%, is taken as a systematic uncertainty.

The effect of modelling of the signal hadronisation is studied comparing the selection efficiencies based on simulated samples with different hadronisation schemes, JETSET [16], HERWIG [13] and ARIADNE [14]. The hadronisation parameters in these models were tuned to describe inclusive hadronic Z decays at $\sqrt{s} = 91$ GeV. No difference is observed for the qqe$\nu(\gamma)$ and qq$\mu\nu(\gamma)$ cross sections and the statistical accuracy of the test, 0.3%, is taken as a systematic uncertainty. In the case of the qq$\tau\nu(\gamma)$ selection, the treatment of hadronic jets and the tight requirements needed in order to identify the τ jet, lead to an uncertainty of 1.1%. In the qqqq(γ) case a larger difference of 1.8%, dominated by the HERWIG comparison, is observed and assigned as the signal hadronisation uncertainty.

The hadronisation systematics due to the $e^+e^- \to q\bar{q}(\gamma)$ background is negligible for qq$\ell\nu$ final states. For the qqqq(γ) selection it is estimated by two methods. In the first, a sample of HERWIG $q\bar{q}(\gamma)$ events is used instead of JETSET events. In the second, data and Monte Carlo distributions of hadronic Z decays collected at $\sqrt{s} = 91$ GeV are compared for the y_{34} variable. The discrepancy is treated by reweighting Monte Carlo events to match the data as a function of y_{34}. The resulting accepted $q\bar{q}(\gamma)$ cross section for a neural network output greater than 0.6 is increased by 4.8% relative to the JETSET prediction, while the signal cross section is decreased by 0.6%. These corrections are applied to the quoted results. From the uncertainty on the reweighting procedure and from the HERWIG−JETSET comparison, a 0.6% systematic uncertainty is assigned.

The modelling of Bose-Einstein correlations between hadrons from W decays may affect the selection efficiencies. In our recent study [29] we have measured the strength of intra-W Bose-Einstein correlations in semileptonic W decays. Its value is significantly different from zero and in good agreement with that for light-quark Z decays and with the LUBOEI [30] BE_{32} and BE_0 predictions. The resulting systematic uncertainty is found to be negligible.

The same study shows that Bose-Einstein correlations between particles originating from different W bosons are strongly disfavoured in qqqq(γ) events. Their strength is restricted to at most 1/4 of the strength as simulated in the BE_0/BE_{32} models with full correlations. The difference in the measured qqqq(γ) cross section obtained by using Monte Carlo samples with intra-W only and with full inter-W correlations is rescaled by 1/4 according to the allowed strength of inter-W correlations. The resulting difference of 0.3% is assigned as a systematic uncertainty. The uncertainty coming from the modelling of intra-W correlations is negligible as for the qq$\ell\nu(\gamma)$ case.

The influence of colour reconnection effects between the two hadronic systems arising in WW $\to$ qqqq(γ) decays are estimated using models implemented in ARIADNE (model 2) and PYTHIA 6.1 (models [31] SK I with reconnection parameter $k = 0.6$, SK II and SK II′). In all cases, the effect on the cross section is at the level of the statistical accuracy of 0.3%, which is then taken as the associated systematic uncertainty.

The total systematic uncertainty on the cross sections is estimated to be in the range 1.5%−2.9%, depending on the final state, from the combination of the above considered sources.

4 Results

The CC03 cross sections σ_i of the ten signal processes i, or equivalently the W-decay branching fractions together with the total W-pair cross section, are determined simultaneously in maximum-likelihood fits [9]. For the qqe$\nu(\gamma)$ and the six $\ell\nu\ell\nu(\gamma)$ final states, where the non-W-pair processes have a significant contribution, the efficiencies are determined within the phase-space cuts described in Section 2.1 and 2.2. The measured four-fermion cross sections are scaled by the conversion factors f_i, listed in Table 4, to obtain the CC03 cross sections.

These factors are given by the ratio of the total CC03 cross section and the four-fermion cross section within phase-space cuts and are calculated with the EXCALIBUR Monte Carlo program.

The SM CC03 predictions are obtained using the GENTLE [32] program and also the new calculations implemented in the RacoonWW [33] and YFSWW3 [34] programs that include full $\mathcal{O}(\alpha)$ electroweak corrections, calculated in the double pole approximation [35]. The new predictions are about 2.5% lower than the GENTLE calculations, and have a reduced theoretical uncertainty of about 0.5% instead of 2% [36]. For numerical comparisons, RacoonWW predictions are used.

4.1 Signal Cross Sections

The ten measured CC03 signal cross sections σ_i are listed in Table 4. They agree well with the SM expectations. The correlations between the measured cross sections, reported in Table 5, arise from non-vanishing off-diagonal terms in the efficiency matrix of Table 1. The systematic uncertainties shown in Table 3 and their correlations are taken into account in the determination of the results.

With the assumption of charged current lepton universality in W decays, the number of free parameters in the fit is reduced to three CC03 cross sections: $\sigma_{\ell\nu\ell\nu}$, $\sigma_{\mathrm{qq}\ell\nu}$, summed over all lepton species, and σ_{qqqq}. Their values at $\sqrt{s} = 188.6$ GeV are determined to be:

$$\begin{aligned} \sigma_{\ell\nu\ell\nu} &= 1.67 \pm 0.14 \pm 0.04 \text{ pb} \\ \sigma_{\mathrm{qq}\ell\nu} &= 7.20 \pm 0.24 \pm 0.08 \text{ pb} \\ \sigma_{\mathrm{qqqq}} &= 7.36 \pm 0.24 \pm 0.18 \text{ pb}\,, \end{aligned} \quad (1)$$

where the first uncertainty is statistical and the second systematic. The correlations between these three results are negligible.

4.2 W-Decay Branching Fractions and W-Pair Cross Section

The W decay branching fractions $B(\mathrm{W} \rightarrow \mathrm{f\bar{f}})$ are derived in a combined fit with the total CC03 W-pair cross section. The sum of the branching fractions is fixed to be unity and their values are combined with our measurements at lower centre-of-mass energies [9] including correlations due to systematic uncertainties. The results are presented in Table 6, both without and with the assumption of charged current lepton universality in W decays. This hypothesis is supported by our results. The values for the assumption of lepton universality are:

$$B(\mathrm{W} \rightarrow \mathrm{qq}) = (68.20 \pm 0.68 \pm 0.33)\ \% \qquad B(\mathrm{W} \rightarrow \ell\nu) = (10.60 \pm 0.23 \pm 0.11)\ \%\,. \quad (2)$$

The relation between the W-decay branching fractions and the six elements V_{ij} of the Cabibbo-Kobayashi-Maskawa quark mixing matrix V_{CKM} [37] not involving the top quark is [4]: $1/B(\mathrm{W} \rightarrow \ell\nu) = 3 + 3\,(1 + \alpha_{\mathrm{s}}(m_{\mathrm{W}})/\pi)\,V^2$. Using $\alpha_{\mathrm{s}}(m_{\mathrm{W}}) = 0.121 \pm 0.002$ as the strong coupling constant, our measurement yields:

$$V^2 \;=\; \sum_{i=\mathrm{u,c};\,j=\mathrm{d,s,b}} |V_{ij}|^2 \;=\; 2.065 \pm 0.064 \pm 0.032\,. \quad (3)$$

Using the current world-average values and uncertainties of the other matrix elements [26], the value of V_{cs} is derived as:

$$|V_{\mathrm{cs}}| \;=\; 1.008 \pm 0.032 \pm 0.016\,. \quad (4)$$

This element is the least known of the two dominant diagonal elements appearing in V^2. The statistical uncertainty includes the uncertainties on α_{s} and the other V_{ij} elements but is dominated by the statistical uncertainty on our measured W-decay branching fractions.

Assuming SM W-decay branching fractions [4], the total W-pair cross section at $\sqrt{s} =$ 188.6 GeV is measured to be:

$$\sigma_{\mathrm{WW}} = 16.24 \pm 0.37 \pm 0.22 \text{ pb} . \quad (5)$$

The measurements reported here are in agreement with recent measurements by other LEP experiments at the same centre-of-mass energy [38]. All our measurements of σ_{WW} are compared with the SM expectation in Figure 5. Good agreement is observed.

Acknowledgements

We wish to express our gratitude to the CERN accelerator divisions for the excellent performance of the LEP machine. We acknowledge the contributions of the engineers and technicians who have participated in the construction and maintenance of this experiment.

References

[1] S. L. Glashow, Nucl. Phys. **22** (1961) 579;
S. Weinberg, Phys. Rev. Lett. **19** (1967) 1264;
A. Salam, in *Elementary Particle Theory*, ed. N. Svartholm, Stockholm, Almquist and Wiksell (1968), 367.

[2] M. Veltman, Nucl. Phys. **B7** (1968) 637;
G.M. 't Hooft, Nucl. Phys. **B35** (1971) 167;
G.M. 't Hooft and M. Veltman, Nucl. Phys. **B44** (1972) 189; Nucl. Phys. **B50** (1972) 318.

[3] D. Bardin *et al.*, Nucl. Phys. (Proc. Suppl.) **B 37** (1994) 148;
F.A. Berends *et al.*, Nucl. Phys. (Proc. Suppl.) **B 37** (1994) 163.

[4] W. Beenakker *et al.*, in *Physics at LEP 2*, Report CERN 96-01 (1996), eds G. Altarelli, T. Sjöstrand, F. Zwirner, Vol. 1, p. 79.

[5] D. Bardin *et al.*, in *Physics at LEP 2*, Report CERN 96-01 (1996), eds G. Altarelli, T. Sjöstrand, F. Zwirner, Vol. 2, p. 3.

[6] The L3 Collaboration, B. Adeva *et al.*, Nucl. Instr. and Meth. **A 289** (1990) 35;
M. Chemarin *et al.*, Nucl. Instr. and Meth. **A 349** (1994) 345;
M. Acciarri *et al.*, Nucl. Instr. and Meth. **A 351** (1994) 300;
G. Basti *et al.*, Nucl. Instr. and Meth. **A 374** (1996) 293;
A. Adam *et al.*, Nucl. Instr. and Meth. **A 383** (1996) 342.

[7] I.C. Brock *et al.*, Nucl. Instr. and Meth. **A 381** (1996) 236.

[8] The L3 Collaboration, M. Acciarri *et al.*, Phys. Lett. **B 479** (2000) 101.

[9] The L3 Collaboration, M. Acciarri *et al.*, Phys. Lett. **B 398** (1997) 223; Phys. Lett. **B 407** (1997) 419; Phys. Lett. **B 436** (1998) 437.

[10] H.J. Daum *et al.*, Z. Phys. **C 8** (1981) 167.

[11] S. Catani *et al.*, Phys. Lett. **B 269** (1991) 432;
S. Bethke *et al.*, Nucl. Phys. **B 370** (1992) 310.

[12] KORALW version 1.33 is used.
S. Jadach *et al.*, Comp. Phys. Comm. **94** (1996) 216;
S. Jadach *et al.*, Phys. Lett. **B 372** (1996) 289.

[13] HERWIG version 5.9 is used.
G. Marchesini and B. Webber, Nucl. Phys. **B 310** (1988) 461;
I.G. Knowles, Nucl. Phys. **B 310** (1988) 571;
G. Marchesini *et al.*, Comp. Phys. Comm. **67** (1992) 465.

[14] L. Lönnblad, Comp. Phys. Comm. **71** (1992) 15.

[15] F.A. Berends, R. Kleiss and R. Pittau, Comp. Phys. Comm. **85** (1995) 437.

[16] PYTHIA versions 5.722 and 6.1 are used.
T. Sjöstrand, *PYTHIA 5.7 and JETSET 7.4 Physics and Manual*, CERN-TH/7112/93 (1993), revised August 1995; Comp. Phys. Comm. **82** (1994) 74; hep-ph/0001032.

[17] S. Jadach, B.F.L. Ward and Z. Wąs, Phys. Lett. **B 449** (1999) 97.

[18] KORALZ version 4.02 is used.
S. Jadach, B.F.L. Ward and Z. Wąs, Comp. Phys. Comm. **79** (1994) 503.

[19] J.H. Field, Phys. Lett. **B 323** (1994) 432;
J.H. Field and T. Riemann, Comp. Phys. Comm. **94** (1996) 53.

[20] BHWIDE version 1.01 is used.
S. Jadach, W. Placzek, B.F.L. Ward, Phys. Rev. **D 40** (1989) 3582, Comp. Phys. Comm. **70** (1992) 305, Phys. Lett. **B 390** (1997) 298.

[21] D. Karlen, Nucl. Phys. **B 289** (1987) 23.

[22] F. A. Berends, P. H. Daverfeldt and R. Kleiss, Nucl. Phys. **B 253** (1985) 441.

[23] PHOJET version 1.05 is used.
R. Engel, Z. Phys. **C 66** (1995) 203; R. Engel and J. Ranft, Phys. Rev. **D 54** (1996) 4244.

[24] The L3 detector simulation is based on GEANT Version 3.15.
R. Brun *et al.*, *GEANT 3*, CERN-DD/EE/84-1 (Revised), 1987.
The GHEISHA program (H. Fesefeldt, RWTH Aachen Report PITHA 85/02 (1985)) is used to simulate hadronic interactions.

[25] Z. Kunszt *et al.*, in *Z Physics at LEP 1*, Report CERN 89-08 (1989), eds G. Altarelli, R. Kleiss, C. Verzegnassi, Vol. 1, p. 385.

[26] C. Caso *et al.*, Eur. Phys. J. **C 3** (1998) 1.

[27] G.J. van Oldenborgh, Nucl. Phys. **B 470** (1996) 71.

[28] E. Barberio and Z. Wąs, Comp. Phys. Comm. **79** (1994) 291;
E. Barberio, B. van Eijk and Z. Wąs, Comp. Phys. Comm. **66** (1991) 115.

[29] The L3 Collaboration, M. Acciarri *et al.*, "Measurement of Bose-Einstein Correlations in $e^+e^- \to W^+W^-$ at $\sqrt{s} \approx 189$ GeV", submitted to Phys. Lett. **B**.

[30] L. Lönnblad and T. Sjöstrand, Eur. Phys. J. **C 2** (1998) 165.

[31] T. Sjöstrand and V. Khoze, Z. Phys. **C 64** (1994) 281; Eur. Phys. J. **C 6** (1999) 271.

[32] GENTLE version 2.0 is used.
D. Bardin *et al.*, Comp. Phys. Comm. **104** (1997) 161.

[33] A. Denner *et al.*, Phys. Lett. **B 475** (2000) 127; hep-ph/0006307.

[34] YFSWW3 version 1.14 is used.
S. Jadach *et al.*, Phys. Rev. **D 54** (1996) 5434; Phys. Lett. **B 417** (1998) 326; Phys. Rev. **D 61** (2000) 113010; hep-ph/0007012.

[35] W. Beenakker, F.A. Berends and A.P. Chapovsky, Nucl. Phys. **B 548** (1999) 3.

[36] M.W. Grünewald *et al.*, hep-ph/0005309.

[37] N. Cabibbo, Phys. Rev. Lett. **10** (1963) 531;
M. Kobayashi and T. Maskawa, Prog. Theor. Phys. **49** (1973) 652.

[38] The DELPHI Collaboration, P. Abreu *et al.*, CERN-EP/2000-035;
The ALEPH Collaboration, R. Barate *et al.*, CERN-EP/2000-052.

The L3 Collaboration:

M.Acciarri,[26] P.Achard,[19] O.Adriani,[16] M.Aguilar-Benitez,[25] J.Alcaraz,[25] G.Alemanni,[22] J.Allaby,[17] A.Aloisio,[28] M.G.Alviggi,[28] G.Ambrosi,[19] H.Anderhub,[48] V.P.Andreev,[6,36] T.Angelescu,[12] F.Anselmo,[9] A.Arefiev,[27] T.Azemoon,[3] T.Aziz,[10] P.Bagnaia,[35] A.Bajo,[25] L.Baksay,[43] A.Balandras,[4] S.V.Baldew,[2] S.Banerjee,[10] Sw.Banerjee,[10] A.Barczyk,[48,46] R.Barillère,[17] P.Bartalini,[22] M.Basile,[9] R.Battiston,[32] A.Bay,[22] F.Becattini,[16] U.Becker,[14] F.Behner,[48] L.Bellucci,[16] R.Berbeco,[3] J.Berdugo,[25] P.Berges,[14] B.Bertucci,[32] B.L.Betev,[48] S.Bhattacharya,[10] M.Biasini,[32] A.Biland,[48] J.J.Blaising,[4] S.C.Blyth,[33] G.J.Bobbink,[2] A.Böhm,[1] L.Boldizsar,[13] B.Borgia,[35] D.Bourilkov,[48] M.Bourquin,[19] S.Braccini,[19] J.G.Branson,[39] F.Brochu,[4] A.Buffini,[16] A.Buijs,[44] J.D.Burger,[14] W.J.Burger,[32] X.D.Cai,[14] M.Capell,[14] G.Cara Romeo,[9] G.Carlino,[28] A.M.Cartacci,[16] J.Casaus,[25] G.Castellini,[16] F.Cavallari,[35] N.Cavallo,[37] C.Cecchi,[32] M.Cerrada,[25] F.Cesaroni,[23] M.Chamizo,[19] Y.H.Chang,[50] U.K.Chaturvedi,[18] M.Chemarin,[24] A.Chen,[50] G.Chen,[7] G.M.Chen,[7] H.F.Chen,[20] H.S.Chen,[7] G.Chiefari,[28] L.Cifarelli,[38] F.Cindolo,[9] C.Civinini,[16] I.Clare,[14] R.Clare,[14] G.Coignet,[4] N.Colino,[25] S.Costantini,[5] F.Cotorobai,[12] B.de la Cruz,[25] A.Csilling,[13] S.Cucciarelli,[32] T.S.Dai,[14] J.A.van Dalen,[30] R.D'Alessandro,[16] R.de Asmundis,[28] P.Déglon,[19] A.Degré,[4] K.Deiters,[46] D.della Volpe,[28] E.Delmeire,[19] P.Denes,[34] F.DeNotaristefani,[35] A.De Salvo,[48] M.Diemoz,[35] M.Dierckxsens,[2] D.van Dierendonck,[2] C.Dionisi,[35] M.Dittmar,[48] A.Dominguez,[39] A.Doria,[28] M.T.Dova,[18,♯] D.Duchesneau,[4] D.Dufournaud,[4] P.Duinker,[2] I.Duran,[40] H.El Mamouni,[24] A.Engler,[33] F.J.Eppling,[14] F.C.Erné,[2] P.Extermann,[19] M.Fabre,[46] M.A.Falagan,[25] S.Falciano,[35,17] A.Favara,[17] J.Fay,[24] O.Fedin,[36] M.Felcini,[48] T.Ferguson,[33] H.Fesefeldt,[1] E.Fiandrini,[32] J.H.Field,[19] F.Filthaut,[17] P.H.Fisher,[14] I.Fisk,[39] G.Forconi,[14] K.Freudenreich,[48] C.Furetta,[26] Yu.Galaktionov,[27,14] S.N.Ganguli,[10] P.Garcia-Abia,[5] M.Gataullin,[31] S.S.Gau,[11] S.Gentile,[35,17] N.Gheordanescu,[12] S.Giagu,[35] Z.F.Gong,[20] G.Grenier,[24] O.Grimm,[48] M.W.Gruenewald,[8] M.Guida,[38] R.van Gulik,[2] V.K.Gupta,[34] A.Gurtu,[10] L.J.Gutay,[45] D.Haas,[5] A.Hasan,[29] D.Hatzifotiadou,[9] T.Hebbeker,[8] A.Hervé,[17] P.Hidas,[13] J.Hirschfelder,[33] H.Hofer,[48] G. Holzner,[48] H.Hoorani,[33] S.R.Hou,[50] Y.Hu,[30] I.Iashvili,[47] B.N.Jin,[7] L.W.Jones,[3] P.de Jong,[2] I.Josa-Mutuberría,[25] R.A.Khan,[18] M.Kaur,[18,◇] M.N.Kienzle-Focacci,[19] D.Kim,[35] J.K.Kim,[42] J.Kirkby,[17] D.Kiss,[13] W.Kittel,[30] A.Klimentov,[14,27] A.C.König,[30] A.Kopp,[47] V.Koutsenko,[14,27] M.Kräber,[48] R.W.Kraemer,[33] W.Krenz,[1] A.Krüger,[47] A.Kunin,[14,27] P.Ladron de Guevara,[25] I.Laktineh,[24] G.Landi,[16] M.Lebeau,[17] A.Lebedev,[14] P.Lebrun,[24] P.Lecomte,[48] P.Lecoq,[17] P.Le Coultre,[48] H.J.Lee,[8] J.M.Le Goff,[17] R.Leiste,[47] P.Levtchenko,[36] C.Li,[20] S.Likhoded,[47] C.H.Lin,[50] W.T.Lin,[50] F.L.Linde,[2] L.Lista,[28] Z.A.Liu,[7] W.Lohmann,[47] E.Longo,[35] Y.S.Lu,[7] K.Lübelsmeyer,[1] C.Luci,[17,35] D.Luckey,[14] L.Lugnier,[24] L.Luminari,[35] W.Lustermann,[48] W.G.Ma,[20] M.Maity,[10] L.Malgeri,[17] A.Malinin,[17] C.Maña,[25] D.Mangeol,[30] J.Mans,[34] G.Marian,[15] J.P.Martin,[24] F.Marzano,[35] K.Mazumdar,[10] R.R.McNeil,[6] S.Mele,[17] L.Merola,[28] M.Meschini,[16] W.J.Metzger,[30] M.von der Mey,[1] A.Mihul,[12] H.Milcent,[17] G.Mirabelli,[35] J.Mnich,[17] G.B.Mohanty,[10] T.Moulik,[10] G.S.Muanza,[24] A.J.M.Muijs,[2] B.Musicar,[39] M.Musy,[35] M.Napolitano,[28] S.Natale,[35] F.Nessi-Tedaldi,[48] H.Newman,[31] T.Niessen,[1] A.Nisati,[35] H.Nowak,[47] R.Ofierzynski,[48] G.Organtini,[35] A.Oulianov,[27] C.Palomares,[25] D.Pandoulas,[1] S.Paoletti,[35,17] P.Paolucci,[28] R.Paramatti,[35] H.K.Park,[33] I.H.Park,[42] G.Passaleva,[17] S.Patricelli,[28] T.Paul,[11] M.Pauluzzi,[32] C.Paus,[17] F.Pauss,[48] M.Pedace,[35] S.Pensotti,[26] D.Perret-Gallix,[4] B.Petersen,[30] D.Piccolo,[28] F.Pierella,[9] M.Pieri,[16] P.A.Piroué,[34] E.Pistolesi,[26] V.Plyaskin,[27] M.Pohl,[19] V.Pojidaev,[27,16] H.Postema,[14] J.Pothier,[17] D.O.Prokofiev,[45] D.Prokofiev,[36] J.Quartieri,[38] G.Rahal-Callot,[48,17] M.A.Rahaman,[10] P.Raics,[15] N.Raja,[10] R.Ramelli,[48] P.G.Rancoita,[26] R.Ranieri,[16] A.Raspereza,[47] G.Raven,[39] P.Razis,[29] D.Ren,[48] M.Rescigno,[35] S.Reucroft,[11] S.Riemann,[47] K.Riles,[3] J.Rodin,[43] B.P.Roe,[3] L.Romero,[25] A.Rosca,[8] S.Rosier-Lees,[4] J.A.Rubio,[17] G.Ruggiero,[16] H.Rykaczewski,[48] S.Saremi,[6] S.Sarkar,[35] J.Salicio,[17] E.Sanchez,[17] M.P.Sanders,[30] M.E.Sarakinos,[21] C.Schäfer,[17] V.Schegelsky,[36] S.Schmidt-Kaerst,[1] D.Schmitz,[1] H.Schopper,[49] D.J.Schotanus,[30] G.Schwering,[1] C.Sciacca,[28] A.Seganti,[9] L.Servoli,[32] S.Shevchenko,[31] N.Shivarov,[41] V.Shoutko,[27] E.Shumilov,[27] A.Shvorob,[31] T.Siedenburg,[1] D.Son,[42] B.Smith,[33] P.Spillantini,[16] M.Steuer,[14] D.P.Stickland,[34] A.Stone,[6] B.Stoyanov,[41] A.Straessner,[1] K.Sudhakar,[10] G.Sultanov,[18] L.Z.Sun,[20] H.Suter,[48] J.D.Swain,[18] Z.Szillasi,[43,¶] T.Sztaricskai,[43,¶] X.W.Tang,[7] L.Tauscher,[5] L.Taylor,[11] B.Tellili,[24] C.Timmermans,[30] Samuel C.C.Ting,[14] S.M.Ting,[14] S.C.Tonwar,[10] J.Tóth,[13] C.Tully,[17] K.L.Tung,[7] Y.Uchida,[14] J.Ulbricht,[48] E.Valente,[35] G.Vesztergombi,[13] I.Vetlitsky,[27] D.Vicinanza,[38] G.Viertel,[48] S.Villa,[11] P.Violini,[35] M.Vivargent,[4] S.Vlachos,[5] I.Vodopianov,[36] H.Vogel,[33] H.Vogt,[47] I.Vorobiev,[27] A.A.Vorobyov,[36] A.Vorvolakos,[29] M.Wadhwa,[5] W.Wallraff,[1] M.Wang,[14] X.L.Wang,[20] Z.M.Wang,[20] A.Weber,[1] M.Weber,[1] P.Wienemann,[1] H.Wilkens,[30] S.X.Wu,[14] S.Wynhoff,[17] L.Xia,[31] Z.Z.Xu,[20] J.Yamamoto,[3] B.Z.Yang,[20] C.G.Yang,[7] H.J.Yang,[7] M.Yang,[7] J.B.Ye,[20] S.C.Yeh,[51] An.Zalite,[36] Yu.Zalite,[36] Z.P.Zhang,[20] G.Y.Zhu,[7] R.Y.Zhu,[31] A.Zichichi,[9,17,18] G.Zilizi,[43,¶] B.Zimmermann,[48] M.Zöller.[1]

1 I. Physikalisches Institut, RWTH, D-52056 Aachen, FRG[§]
III. Physikalisches Institut, RWTH, D-52056 Aachen, FRG[§]
2 National Institute for High Energy Physics, NIKHEF, and University of Amsterdam, NL-1009 DB Amsterdam, The Netherlands
3 University of Michigan, Ann Arbor, MI 48109, USA
4 Laboratoire d'Annecy-le-Vieux de Physique des Particules, LAPP,IN2P3-CNRS, BP 110, F-74941 Annecy-le-Vieux CEDEX, France
5 Institute of Physics, University of Basel, CH-4056 Basel, Switzerland
6 Louisiana State University, Baton Rouge, LA 70803, USA
7 Institute of High Energy Physics, IHEP, 100039 Beijing, China[△]
8 Humboldt University, D-10099 Berlin, FRG[§]
9 University of Bologna and INFN-Sezione di Bologna, I-40126 Bologna, Italy
10 Tata Institute of Fundamental Research, Bombay 400 005, India
11 Northeastern University, Boston, MA 02115, USA
12 Institute of Atomic Physics and University of Bucharest, R-76900 Bucharest, Romania
13 Central Research Institute for Physics of the Hungarian Academy of Sciences, H-1525 Budapest 114, Hungary[‡]
14 Massachusetts Institute of Technology, Cambridge, MA 02139, USA
15 KLTE-ATOMKI, H-4010 Debrecen, Hungary[¶]
16 INFN Sezione di Firenze and University of Florence, I-50125 Florence, Italy
17 European Laboratory for Particle Physics, CERN, CH-1211 Geneva 23, Switzerland
18 World Laboratory, FBLJA Project, CH-1211 Geneva 23, Switzerland
19 University of Geneva, CH-1211 Geneva 4, Switzerland
20 Chinese University of Science and Technology, USTC, Hefei, Anhui 230 029, China[△]
21 SEFT, Research Institute for High Energy Physics, P.O. Box 9, SF-00014 Helsinki, Finland
22 University of Lausanne, CH-1015 Lausanne, Switzerland
23 INFN-Sezione di Lecce and Universitá Degli Studi di Lecce, I-73100 Lecce, Italy
24 Institut de Physique Nucléaire de Lyon, IN2P3-CNRS,Université Claude Bernard, F-69622 Villeurbanne, France
25 Centro de Investigaciones Energéticas, Medioambientales y Tecnologícas, CIEMAT, E-28040 Madrid, Spain[♭]
26 INFN-Sezione di Milano, I-20133 Milan, Italy
27 Institute of Theoretical and Experimental Physics, ITEP, Moscow, Russia
28 INFN-Sezione di Napoli and University of Naples, I-80125 Naples, Italy
29 Department of Natural Sciences, University of Cyprus, Nicosia, Cyprus
30 University of Nijmegen and NIKHEF, NL-6525 ED Nijmegen, The Netherlands
31 California Institute of Technology, Pasadena, CA 91125, USA
32 INFN-Sezione di Perugia and Universitá Degli Studi di Perugia, I-06100 Perugia, Italy
33 Carnegie Mellon University, Pittsburgh, PA 15213, USA
34 Princeton University, Princeton, NJ 08544, USA
35 INFN-Sezione di Roma and University of Rome, "La Sapienza", I-00185 Rome, Italy
36 Nuclear Physics Institute, St. Petersburg, Russia
37 INFN-Sezione di Napoli and University of Potenza, I-85100 Potenza, Italy
38 University and INFN, Salerno, I-84100 Salerno, Italy
39 University of California, San Diego, CA 92093, USA
40 Dept. de Fisica de Particulas Elementales, Univ. de Santiago, E-15706 Santiago de Compostela, Spain
41 Bulgarian Academy of Sciences, Central Lab. of Mechatronics and Instrumentation, BU-1113 Sofia, Bulgaria
42 Laboratory of High Energy Physics, Kyungpook National University, 702-701 Taegu, Republic of Korea
43 University of Alabama, Tuscaloosa, AL 35486, USA
44 Utrecht University and NIKHEF, NL-3584 CB Utrecht, The Netherlands
45 Purdue University, West Lafayette, IN 47907, USA
46 Paul Scherrer Institut, PSI, CH-5232 Villigen, Switzerland
47 DESY, D-15738 Zeuthen, FRG
48 Eidgenössische Technische Hochschule, ETH Zürich, CH-8093 Zürich, Switzerland
49 University of Hamburg, D-22761 Hamburg, FRG
50 National Central University, Chung-Li, Taiwan, China
51 Department of Physics, National Tsing Hua University, Taiwan, China
§ Supported by the German Bundesministerium für Bildung, Wissenschaft, Forschung und Technologie
‡ Supported by the Hungarian OTKA fund under contract numbers T019181, F023259 and T024011.
¶ Also supported by the Hungarian OTKA fund under contract numbers T22238 and T026178.
♭ Supported also by the Comisión Interministerial de Ciencia y Tecnología.
♯ Also supported by CONICET and Universidad Nacional de La Plata, CC 67, 1900 La Plata, Argentina.
♢ Also supported by Panjab University, Chandigarh-160014, India.
△ Supported by the National Natural Science Foundation of China.

Selection	Efficiencies [%] for									
	$e\nu e\nu$	$e\nu\mu\nu$	$e\nu\tau\nu$	$\mu\nu\mu\nu$	$\mu\nu\tau\nu$	$\tau\nu\tau\nu$	$qqe\nu$	$qq\mu\nu$	$qq\tau\nu$	qqqq
$e^+e^- \to e\nu e\nu(\gamma)$	64.2	0.3	12.6	—	—	1.1				
$e^+e^- \to e\nu\mu\nu(\gamma)$	—	60.6	10.0	0.5	10.8	1.7				
$e^+e^- \to e\nu\tau\nu(\gamma)$	5.3	1.1	36.8	—	0.1	7.1				
$e^+e^- \to \mu\nu\mu\nu(\gamma)$	—	—	—	50.6	8.7	0.8				
$e^+e^- \to \mu\nu\tau\nu(\gamma)$	—	2.9	0.2	2.2	31.6	4.7				
$e^+e^- \to \tau\nu\tau\nu(\gamma)$	0.1	0.1	1.3	—	0.8	19.8				
$e^+e^- \to qqe\nu(\gamma)$							81.5	0.3	1.7	—
$e^+e^- \to qq\mu\nu(\gamma)$							0.2	76.7	3.6	—
$e^+e^- \to qq\tau\nu(\gamma)$							5.3	6.5	50.6	0.3
$e^+e^- \to qqqq(\gamma)$							0.2	—	0.8	87.2

Table 1: Selection efficiencies for signal processes $e^+e^- \to \ell\nu\ell\nu(\gamma)$, $e^+e^- \to qq\ell\nu(\gamma)$, and $e^+e^- \to qqqq(\gamma)$. For the $\ell\nu\ell\nu$ and $qqe\nu$ selections, the signal efficiencies are derived from a CC56+NC56 and a CC20 Monte Carlo sample, respectively, and given within phase-space cuts. The total efficiencies at CC03 level for the $\ell\nu\ell\nu$ and $qqe\nu$ selections are 52.3% and 78.1%, respectively. For the qqqq selection, the numbers are quoted for a neural-network output larger than 0.6.

Selection	N_{data}	N_{bg}
$\mathrm{e^+e^-} \to \mathrm{e}\nu\mathrm{e}\nu(\gamma)$	49	9.4 ± 3.0
$\mathrm{e^+e^-} \to \mathrm{e}\nu\mu\nu(\gamma)$	43	4.2 ± 0.7
$\mathrm{e^+e^-} \to \mathrm{e}\nu\tau\nu(\gamma)$	38	2.3 ± 0.7
$\mathrm{e^+e^-} \to \mu\nu\mu\nu(\gamma)$	24	8.3 ± 0.9
$\mathrm{e^+e^-} \to \mu\nu\tau\nu(\gamma)$	26	0.9 ± 0.2
$\mathrm{e^+e^-} \to \tau\nu\tau\nu(\gamma)$	10	1.1 ± 0.4
$\mathrm{e^+e^-} \to \mathrm{qqe}\nu(\gamma)$	363	14.8 ± 0.9
$\mathrm{e^+e^-} \to \mathrm{qq}\mu\nu(\gamma)$	340	13.8 ± 0.7
$\mathrm{e^+e^-} \to \mathrm{qq}\tau\nu(\gamma)$	329	41.7 ± 0.7
$\mathrm{e^+e^-} \to \mathrm{qqqq}(\gamma)$	1431	266.6 ± 1.2

Table 2: Number of selected data events, N_{data}, and number of expected non-WW background events, N_{bg}, for the different selections. The uncertainties include only the Monte Carlo statistics. For the qqqq selection, the numbers are quoted for a neural-network output larger than 0.6.

Systematic Uncertainties on σ [%]					
	Final State				
Source	$\ell\nu\ell\nu$	$\mathrm{qqe}\nu$	$\mathrm{qq}\mu\nu$	$\mathrm{qq}\tau\nu$	qqqq
Luminosity	0.2				
MC statistics (signal)	0.6	0.2	0.3	0.5	0.5
MC statistics (background)	2.0	0.1	0.2	0.4	0.1
Selection procedure	1.4	1.2	1.3	2.5	1.1
Background cross sections	< 0.1	0.1	0.3	0.3	0.2
W mass (± 0.10 GeV)	0.3	0.1	0.1	0.2	0.1
W width (± 0.06 GeV)	0.2	0.1	< 0.1	0.1	< 0.1
ISR simulation	0.2	< 0.1			
FSR simulation	0.4	0.9	0.7	0.3	0.2
CC03 versus 4F	—	—	0.1	0.1	0.4
Hadronisation (signal)	—	0.3	0.3	1.1	1.8
Hadronisation (background)	—	—	—	—	0.6
Bose-Einstein effects	—	< 0.1			0.3
Colour Reconnection	—	—	—	—	0.3
Total	2.6	1.5	1.6	2.9	2.3

Table 3: Contributions to the systematic uncertainty on the cross section measurements. The systematic uncertainties are relative to the cross sections listed in Table 4.

Process	Conversion factor f	σ(CC03) [pb]	σ_{SM} [pb]
$\mathrm{e^+e^-} \rightarrow \mathrm{e}\nu\mathrm{e}\nu(\gamma)$	0.88	$0.22 \pm 0.06 \pm 0.01$	0.19
$\mathrm{e^+e^-} \rightarrow \mathrm{e}\nu\mu\nu(\gamma)$	1.07	$0.22 \pm 0.07 \pm 0.01$	0.37
$\mathrm{e^+e^-} \rightarrow \mathrm{e}\nu\tau\nu(\gamma)$	1.07	$0.50 \pm 0.11 \pm 0.01$	0.37
$\mathrm{e^+e^-} \rightarrow \mu\nu\mu\nu(\gamma)$	0.96	$0.10 \pm 0.06 \pm 0.01$	0.19
$\mathrm{e^+e^-} \rightarrow \mu\nu\tau\nu(\gamma)$	1.10	$0.43 \pm 0.11 \pm 0.01$	0.37
$\mathrm{e^+e^-} \rightarrow \tau\nu\tau\nu(\gamma)$	0.96	$0.20 \pm 0.09 \pm 0.01$	0.19
$\mathrm{e^+e^-} \rightarrow \mathrm{qqe}\nu(\gamma)$	1.01	$2.39 \pm 0.13 \pm 0.04$	2.37
$\mathrm{e^+e^-} \rightarrow \mathrm{qq}\mu\nu(\gamma)$	—	$2.27 \pm 0.14 \pm 0.04$	2.37
$\mathrm{e^+e^-} \rightarrow \mathrm{qq}\tau\nu(\gamma)$	—	$2.64 \pm 0.21 \pm 0.08$	2.37
$\mathrm{e^+e^-} \rightarrow \mathrm{qqqq}(\gamma)$	—	$7.36 \pm 0.24 \pm 0.18$	7.41

Table 4: Conversion factors and cross sections of four-fermion final states. The ratio f of the CC03 cross section without cuts and the four-fermion cross section within phase-space cuts is calculated with EXCALIBUR and listed in the second column. The third column shows the measured CC03 cross sections, σ(CC03). The qqqq cross section is obtained from a fit to the neural-network output distribution as described in Section 2.3. The first uncertainty is statistical and the second systematic. Also shown are the SM predictions for the cross sections, σ_{SM}.

Correlation coefficients										
	$e\nu e\nu$	$e\nu\mu\nu$	$e\nu\tau\nu$	$\mu\nu\mu\nu$	$\mu\nu\tau\nu$	$\tau\nu\tau\nu$	$qqe\nu$	$qq\mu\nu$	$qq\tau\nu$	qqqq
$e\nu e\nu$	+1.00	+0.09	−0.37	0.00	−0.01	+0.05				
$e\nu\mu\nu$		+1.00	−0.27	+0.09	−0.31	+0.07				
$e\nu\tau\nu$			+1.00	−0.01	+0.05	−0.25				
$\mu\nu\mu\nu$				+1.00	−0.32	+0.03				
$\mu\nu\tau\nu$					+1.00	−0.18				
$\tau\nu\tau\nu$						+1.00				
$qqe\nu$							+1.00	0.00	−0.10	0.00
$qq\mu\nu$								+1.00	−0.15	0.00
$qq\tau\nu$									+1.00	−0.01
qqqq										+1.00

Table 5: Correlation coefficients between the cross section measurements of single channels.

Parameter	Lepton Non-Universality	Lepton Universality	Standard Model
$B(\mathrm{W} \to \mathrm{e}\nu)$ [%]	$10.77 \pm 0.45 \pm 0.16$	—	—
$B(\mathrm{W} \to \mu\nu)$ [%]	$9.90 \pm 0.46 \pm 0.15$	—	—
$B(\mathrm{W} \to \tau\nu)$ [%]	$11.24 \pm 0.62 \pm 0.22$	—	—
$B(\mathrm{W} \to \ell\nu)$ [%]	—	$10.60 \pm 0.23 \pm 0.11$	10.83
$B(\mathrm{W} \to \mathrm{qq})$ [%]	$68.09 \pm 0.69 \pm 0.33$	$68.20 \pm 0.68 \pm 0.33$	67.51
σ_{WW} [pb]	$16.29 \pm 0.37 \pm 0.22$	$16.22 \pm 0.37 \pm 0.21$	16.24

Table 6: W-decay branching fractions, B, and total W-pair cross section, σ_{WW}, derived without and with the assumption of charged-current lepton universality. The correlations between the leptonic branching fractions are −0.03, −0.28 and −0.29 for $\mathrm{e}\mu$, $\mathrm{e}\tau$ and $\mu\tau$, respectively. Also shown are the W-decay branching fractions [4] and the total W-pair cross section as expected in the SM.

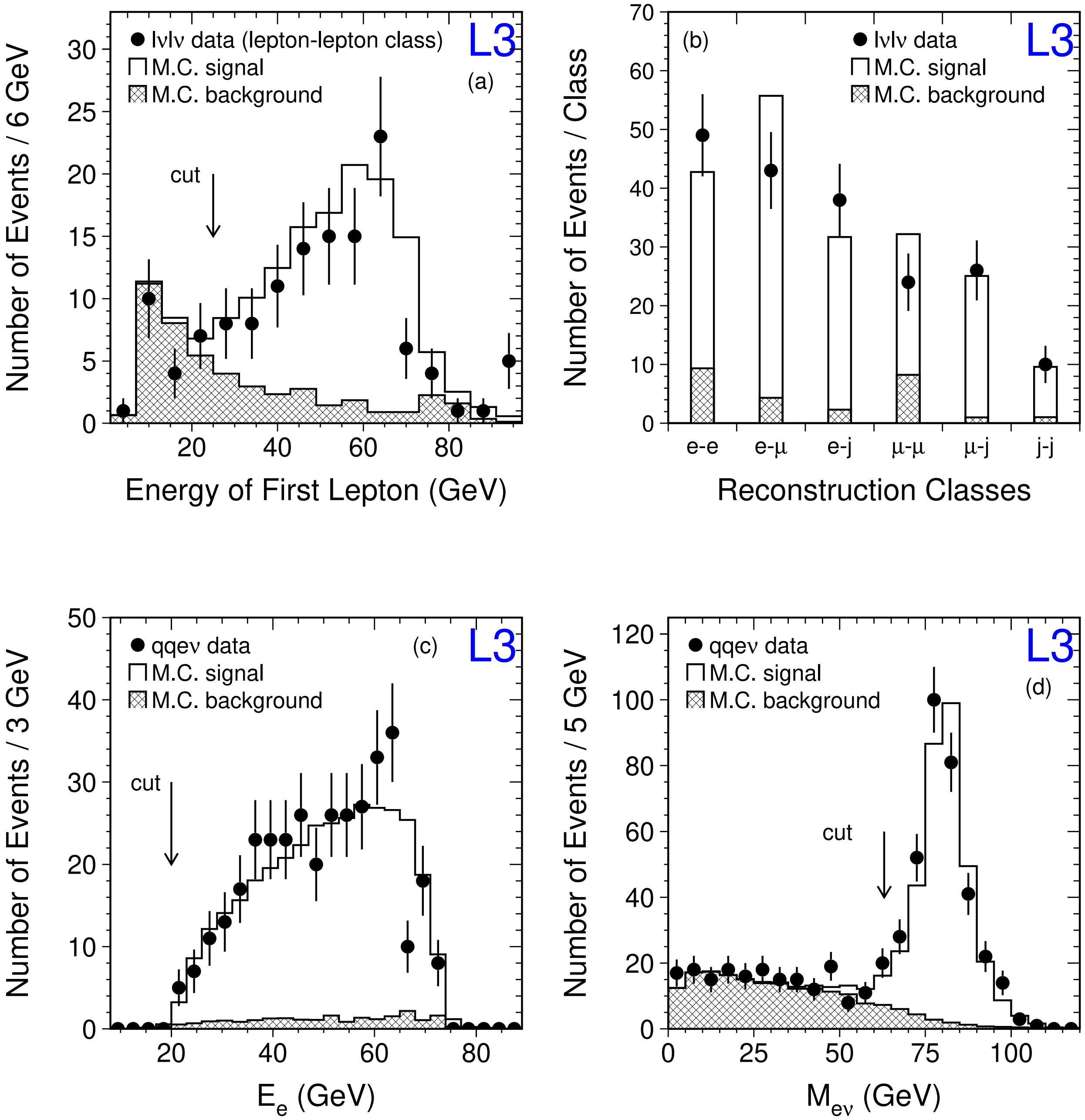

Figure 1: Comparison of data and Monte Carlo distributions of variables used in the $e^+e^- \to \ell\nu\ell\nu(\gamma)$ and $e^+e^- \to qqe\nu(\gamma)$ selections. The background consists of non-$\ell\nu\ell\nu$/qqeν processes. (a) The energy of the most energetic electron or muon in the lepton-lepton class. The vertical arrow indicates the cut position. The events in the plots have passed all other cuts. (b) The number of events in each final state topology (e=electron, μ=muon, j= hadronic τ-jet) after all cuts. (c) The energy, E_e, of the electrons identified in the BGO calorimeter. (d) The invariant mass, $M_{e\nu}$, of the electron-neutrino system.

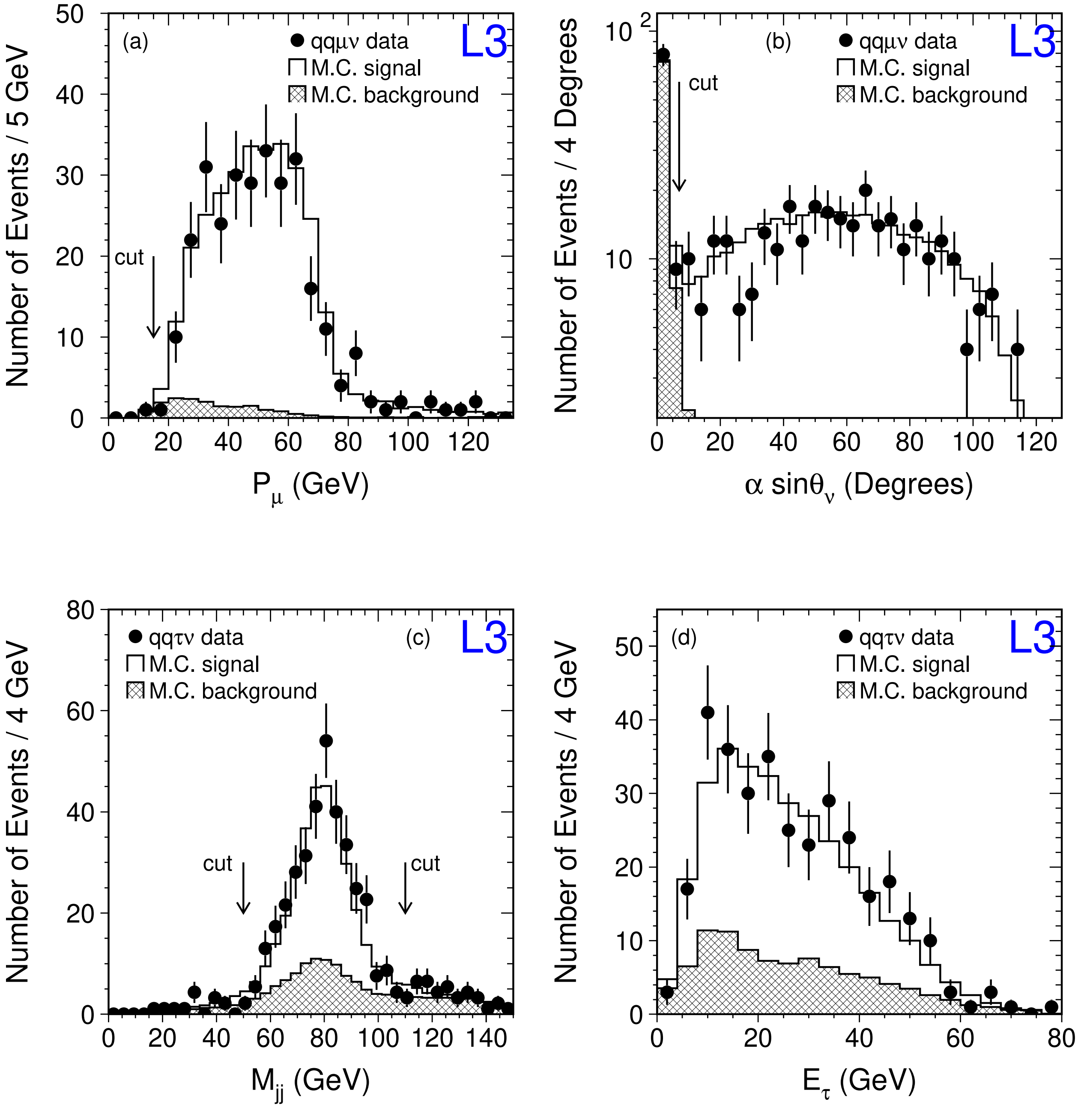

Figure 2: Comparison of data and Monte Carlo distributions of variables used in the $e^+e^- \to qq\mu\nu(\gamma)$ and $e^+e^- \to qq\tau\nu(\gamma)$ selections. (a) The momentum, P_μ, of the muons reconstructed in the muon chambers. (b) The variable $\alpha \sin\theta_\nu$ described in the text. (c) The invariant mass, M_{jj}, of the jet-jet system. (d) The energy, E_τ, of the visible decay products of the τ.

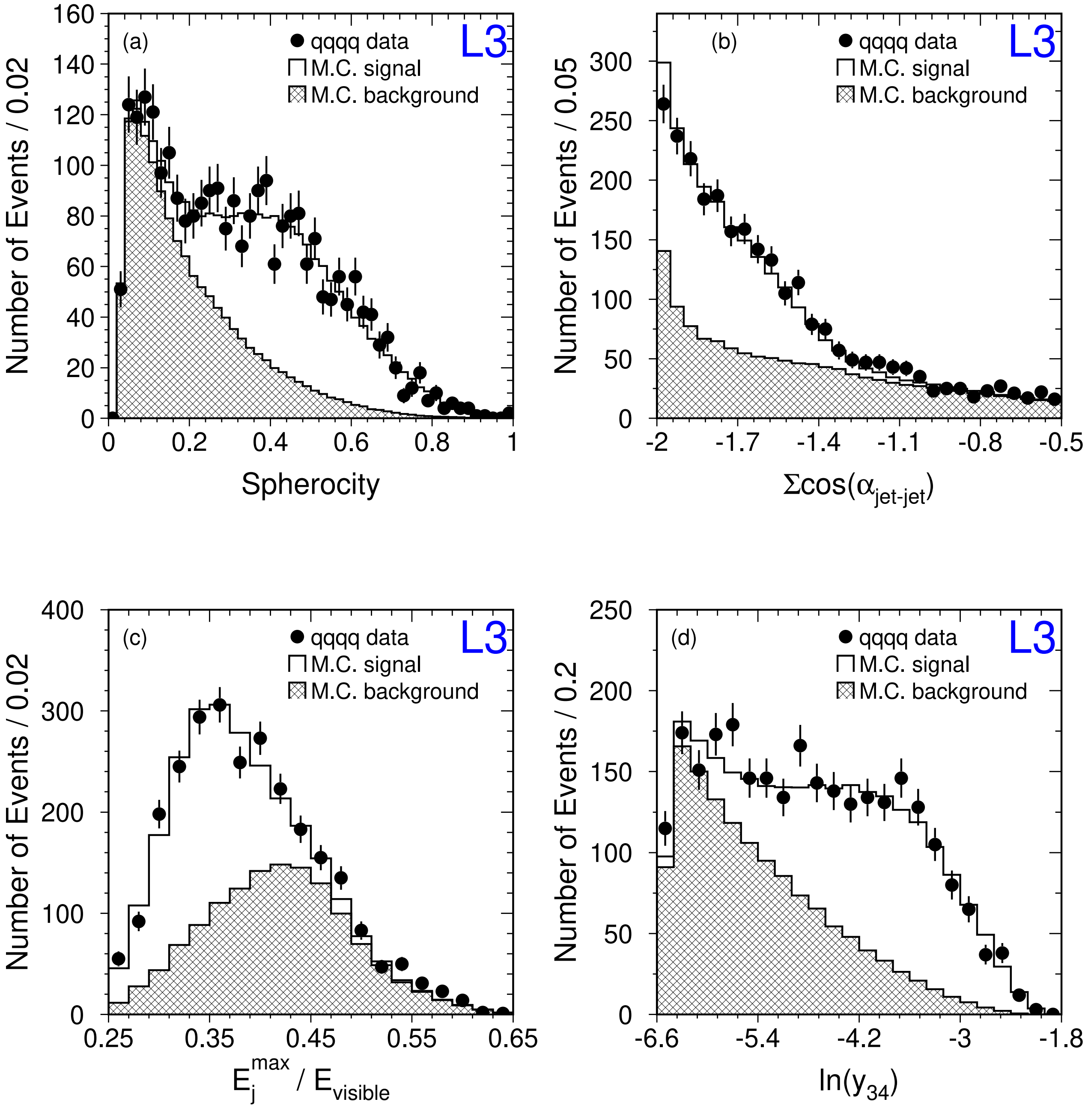

Figure 3: Distributions of input variables for the neural network used in the analysis of the $e^+e^- \rightarrow qqqq(\gamma)$ process. All selection cuts are applied. (a) The spherocity. (b) The sum of cosines of the jet-jet angles. (c) The maximal jet energy, E_j^{max}, normalised to the total visible energy. (d) The quantity $\ln(y_{34})$.

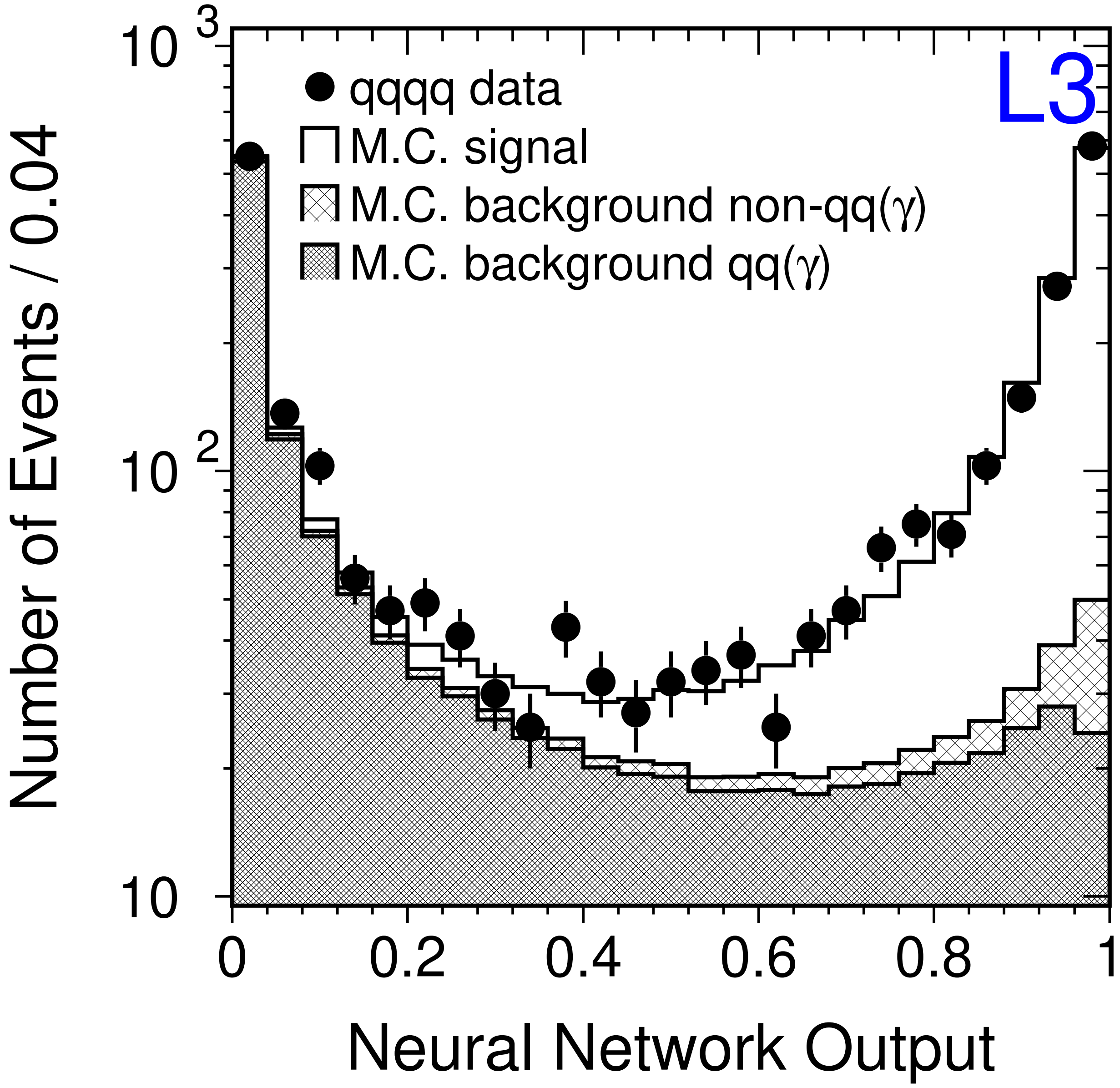

Figure 4: Comparison of data and Monte Carlo distributions of the neural network output for selected $e^+e^- \rightarrow qqqq(\gamma)$ events.

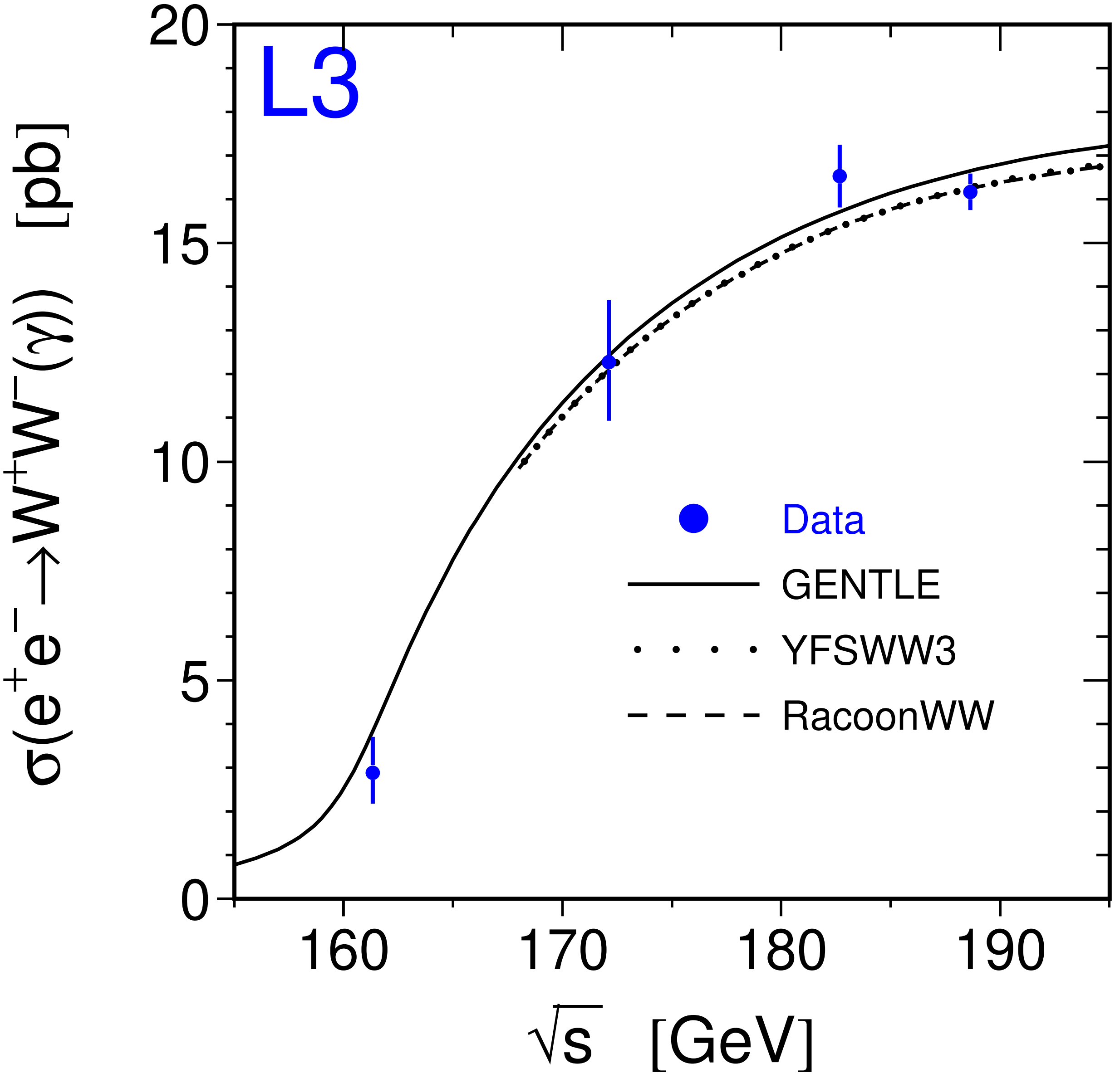

Figure 5: The CC03 cross section of the process $e^+e^- \rightarrow W^+W^-(\gamma)$ as a function of the centre-of-mass energy. The published measurements at $\sqrt{s} = 161$, 172 and 183 GeV, and the new measurement at $\sqrt{s} = 189$ GeV are shown combining statistical and systematic uncertainties in quadrature. The curves show the SM expectation according to different calculations.